Supplementary Information for

Tartaric acid-derived chiral carbon nanodots for catalytic enantioselective ring-opening reactions of styrene oxide

Xinyi Zhao,[a] Yana Reva,[b] Bikash Jana,[b,d] Daniel Langford,[b] Marina Kinzelmann,[e] Zhipeng Zhang,[a] Qi Liu,*[a] Thomas Drewello,[e] Dirk M. Guldi,*[b] Xiaoqing Chen,*[a,c]

[a] College of Chemistry and Chemical Engineering, Central South University, Changsha 410083, Hunan, China

[b] Department of Chemistry and Pharmacy & Interdisciplinary Center for Molecular Materials (ICMM), Physical Chemistry I, Friedrich-Alexander-Universität Erlangen-Nürnberg, Egerlandstraße 3, 91058 Erlangen, Germany

[c] Key Laboratory of Hunan Province for Water Environment and Agriculture Product Safety, Central South University, Changsha 410083, Hunan, China

[d] Technion – Israel Institute of Technology, Schulich Faculty of Chemistry, Technion, 3200008 Haifa, Israel

[e] Department of Chemistry and Pharmacy, Physical Chemistry I, Friedrich-Alexander-Universität Erlangen-Nürnberg, Egerlandstraße 3, 91058 Erlangen, Germany

*Corresponding author: Tel: +86-731-88830833

E-mail address: iliuqi@csu.edu.cn (Qi Liu), dirk.guldi@fau.de (Dirk M. Guldi), xqchen@csu.edu.cn (Xiaoqing Chen)

Content of Supplementary Information:

1. Chemicals and reagents

L-(+)-tartaric acid (L-TA, ACS reagent grade), D-(–)-tartaric acid (D-TA, 99%), ethylenediamine (EDA, 99.5%), sulfanilic acid (SA, ACS reagent grade), p-toluenesulfonic acid monohydrate (PTSA, 99%), styrene oixide (SO, 97%), 2-methoxy-2-phenylethanol (MP, 99%), (*R*)-(–)-2-methoxy-2-phenylethanol ((*R*)- (–)- MP, ee: 98%), sodium chloride (NaCl, 99%), and potassium chloride (KCl, 99%) used in this work were all from Sigma-Aldrich Chemie GmbH (Taufkirchen, Germany). (*R*)- (–)- SO (ee: 97%) and (*S*)- (+)- SO (ee: 98%) were brought from Aladdin Bio-Chem Technology Co., Ltd (Shanghai, China). Additionally, potassium dihydrogen phosphate (KH_2PO_3, Merk), dipotassium hydrogen phosphate (K_2HPO_3, Fluka, 98%), sodium citrate dehydrate (Fluka, 99%) and citric acid monohydrate (Sigma Aldrich, ACS reagent grade) were used for the buffer preparation. 4-(Methylsulfonyl)aniline (MSA, 98%) were bought from Tokyo Chemical Industry Co., Ltd. Deutschland GmbH (Frankfurt, Germany) and nitrobenzene (NB, 99.5%) were obtained from Thermo Fisher Scientific (Massachusetts, USA). Methanol (technical grade) was utilized for reaction. All aqueous solutions were prepared using ultrapure water (≥ 18 MΩ/cm, Milli-Q water purification system, Millipore).

2. Instruments

FT-IR spectra were carried out on a Shimadzu (IRPrestige 21) (ATR device) spectrometer and Raman spectra were gained on a WiTec alpha 300r confocal Raman microscope with a HeNe laser. Perkin Elmer Lambda 2 spectrometer or Perkin Elmer Lambda 35 spectrophotometer were introduced for UV-vis measurements. The fluorescence and 3D fluorescence were conducted with a Fluoromax 3 spectrometer spectrofluorometer (Horiba Yobin Yvon). NMR experiments were carried out in a Magritek Spinsolve Carbon SPA520 43 MHz. The light source was a 150 W Xe lamp (Newport Corporation) and the light intensities were tuned around 100 mW/cm^2. Catalytical performance was quantified through a gas chromatography (GC) setup (Bruker 430-GC) connected with FactorFour Capillary Column from Varian (VF-5ms, 30 m×25 mm). Mass spectrometry was measured *via* a quadrupole time-of-flight (qToF) mass spectrometer (micrOTOF-Q II, Bruker) with an electrospray ionization source. Electronic circular dichroism (ECD) spectra were analyzed by JASCO J815 CD Spectrometer under 20 ℃ and 3 L/min of N_2.

3. Synthesis of L/D-TASA CNDs and the other chiral CNDs

L/D-TASA CNDs were prepared by mixing two precursors, L- (+)- tartaric acid (L-TA) or D- (–)- tartaric acid (D-TA) (1 mmol) and sulfanilic acid (SA) (2 mmol) dissolved in 10 mL pure water and subsequently transferred into a 50-mL Teflon lined stainless steel autoclave and then heated to 180 ℃ for 6 h. After slowly cooling to room temperature, the obtained chiral products were filtered through micropore film (0.22 μm) and dialyzed against ultrapure water through a dialysis membrane (MWAG of 500 Da) for 24 h. After being dried and weighed, the purified L/D-TASA CNDs were subsequently prepared into the solution with the concentration of 600 μg/mL, which were stored at 4 ℃ for further use.

In order to explore the preparation process and catalytic reaction mechanism, different precursors were selected *via* the same preparation method mentioned above, and corresponding chiral CNDs were named as shown in **Table S1**. Specially, as precursors of chiral CNDs, the initial concentrations of L/D-TA, PTSA, and MSA were 0.1 mol/L, 0.2 mol/L and 0.2 mol/L respectively. Besides, the solutions of the other purified chiral CNDs for control experiments (600 μg/mL) were obtained accordingly.

4. Characterizations of L/D-TASA CNDs

The elemental composition and functional groups of TASA CNDs were analyzed by X-ray photoelectron spectroscopy (XPS). As Fig. S2a† illustrates the high-resolution C_{1s} spectrum shows three main features at 284.4, 285.7, and 288.9 eV, corresponding to C–C/C=C, O–C, and O=C–N, respectively.[1] In addition, 533.4 and 531.8 eV features are discernable in the high-resolution O_{1s} spectrum (Fig. S2b†). According to the literature, the strongest binding energy relates to C=O followed by C–O.[2] The two fingerprints at 400.5 (C–N) and 401.5 eV (N–H) in the high-resolution N_{1s} spectrum (Fig. S2c†), as well as those at 168.8 ($S_{2p1/2}$, C–S) and 168.0 eV ($S_{2p3/2}$, C–S) in the high-resolution S_{2p} spectrum (Fig. S2d†) corroborate the successful preparation of TASA CNDs.[3, 4]

We continued the structural investigation by means of Raman spectra and Fourier transform infrared spectroscopy (FTIR). The Raman spectra in Fig. S3a† prompt to the disorder of the carbon-skeleton. In particular, existence of defective or disordered structure stems from the D-band at 1357 cm^{-1} and some ordered regions were concluded from the G-band at 1580 cm^{-1}. Besides, the D-to-G intensity ratio is 0.9 for D-TASA CNDs, while it is 0.6 for L-TASA CNDs. In other words, D-TASA CNDs are more amorphous than L-TASA CNDs.[5] As far as the FTIR spectra in Fig. S3b† are concerned, features at 2930, 1590, 1485 and 1417 cm^{-1} are distinct for both CNDs. Among them, the 2930 cm^{-1} characteristic indicates the presence of C–H vibrations, while the 1590, 1485, and 1417 cm^{-1} fingerprints are associated with the C–C/C–N stem from vibrations of the aromatic nucleus.[6] Moreover, the carbonyl functionalities are identified through the sharp C=O (1643 cm^{-1}) and C–O–H (1411 cm^{-1}) in-plane blending vibrations.[7] Additionally, 1174 cm^{-1} and 1033 cm^{-1} vibrations originate from C–S and C–SO_3 bonds within the CNDs structures, respectively.[8] The 670 cm^{-1} feature in the L/D-TASA CNDs reflects the C–S bending.

In addition, we evaluated the structure of CNDs by electrospray ionization mass spectrometry (ESI-MS). Fig. S5a-d† documents that TA and SA transform after the thermal preparation processing of CNDs. To this end, the mass spectra of chiral CNDs featured *m/z* 338 and 675 (MS^1) support the presence of molecular chromophores within the structure of CNDs. In previous work, we documented that the presence of tartaric acid leads in the solvothermal synthesis at 180 °C to the formation of a

polymeric matrix (shown in Scheme S1†). The latter is the primary backbone of the CND and enables the intercalation of molecular chromophores.[8, 9] The molecular chromophores, on the other hand, are a product of the amidation reaction with the subsequent ammonia attachment to the backbone of citric acid. Ammonia stemmed from the thermal decomposition of formamide.[9] Hence, we propose the formation of chromophore M within the CNDs. Key is the thermally favorable amidation reaction between TA and SA and subsequent addition of three equivalents of ammonia. SA decomposes at the high reaction temperature and releases ammonia. All of the aforementioned is in good agreement with the FTIR and XPS findings (*vide supra*).

4. Feasibility analysis of ring-opening reaction catalyzed by L/D-TASA CNDs

For the feasibility investigation, 120 μL SO and 1.8 mL methanol were added into 4 mL cuvette and stirred in the stirred tank reactor at room temperature. Then, 450 μL L/D-TASA CNDs aqueous solution was added and reacted for 10 min. Notably, the cuvette was sealed with rubber septum after adding chiral CNDs and the cuvette was kept in the dark conditions all the time. Eventually, the reaction was stopped instantly, and the sample was quickly injected into gas chromatograph (GC) with a flame ionization detector (FID) and FactorFour capillary column (VF-5ms, 30 m×25 mm) by automatic sampler for further analysis. More details of chromatographic conditions were as follows: nitrogen as the carrier gas with 2 mL/min flow rate; injection volume 1.0 μL; and detector temperature 250 ℃. The oven temperature was programmed initially heating at 50 ℃ for 5 min, followed by heating to 120 ℃ at 10 ℃/min (hold for 5 min), and finally to 275 ℃ at 10 ℃/min (hold for 5 min) with the total analysis time of ca. 37.5 min. In addition, SO, MP, and L/D-TASA CNDs under the same conditions served as control groups. All experiments were independently repeated for three times (n = 3).

Next, we performed ring-opening reaction, transforming SO to MP, using L/D-TASA CNDs as a catalyst. The reaction was primarily controlled by GC. In the GC spectra (Fig. S6a†), the reactant SO and product MP were noted at 8.9 min and 11.4 min, respectively. When SO was treated with L/D- TASA CNDs, SO disappeared, while the newly evolving MP indicated the efficiently catalyzed ring-opening reaction. Consistently, a similar trend was observed in hydrogen nuclear magnetic resonance (^{1}H-NMR), in which some of the MP characteristics (3.2, 3.5, and 3.7 ppm) appeared upon the catalytic reaction with CNDs (Fig. S6b†). Overall, we have affirmed the successful catalytic performance of L/D-TASA CNDs in the ring-opening reaction.

5. Optimize the catalytic reaction conditions

The optimal reaction conditions were explored as follows. Initially, the effect of reaction time on catalytic performance was investigated. 120 μL SO and 1.8 mL methanol were added into 4 mL cuvette and stirred in the stirred tank reactor at room temperature. Then, 450 μL L/D-TASA CNDs aqueous solution was added and reacted for a period of time (0, 1, 5, 10, 60 min). Notably, the cuvette was sealed with rubber plug after adding chiral CNDs and the cuvette was wrapped in tin foil in the dark conditions all the time. Eventually, after the reactions, the samples were analyzed by GC with a FID detector under the same condition mentioned above.

Then, in order to explore the effect of reactant concentration on catalytic performance, series of concentration of SO was chosen (40, 80, 160, 200, 240, 320, 400, 480, 600, 800 mM), but kept the other conditions unchanged. In addition, the influence of concentration of catalyst on ring-opening reaction was studied by only changing the concentration of chiral CNDs (1, 3, 5, 10, 20, 30, 40, 45, 50, 100, 200, 300, 400, 450 μg/mL). During the GC analysis, nitrobenzene (NB) was selected as the internal standard, and the internal standard method was used to quantify the product of ring-opening reaction. According to the following formula, conversion rate was calculated.

$$Conversion = \frac{C_0 - C}{C_0} \times 100\% \quad \text{(Eq. 1)}$$

The results of catalytic reaction conditions were discussed as follows. With the increase of reaction time, a marked increase of the generation of MP is observed, and the reaction reaches equilibrium after 10 min (Fig. S7a†). Thereafter, 10 min was selected as the optimal reaction time. Likewise, the reactions under different concentrations of SO and L-TASA CNDs were tested, and eventually found that their optimal concentrations were 480 mM and 300 μg/mL, respectively (Fig. S7b-c†). In short, the optimum reaction conditions were 10 min reaction time with 480 mM SO and 300 μg/mL L/D-TASA CNDs. Under these conditions the catalytic efficiencies were 99.2% and 98.3%, respectively.

6. Chirality analysis of CNDs and catalytic reaction by ECD

Circular dichroism was used to characterize the chirality of ring-opening reaction catalyzed by different chiral CNDs under the optimal reaction conditions (L/D-TA CNDs, L/D-TASA CNDs, L/D-TAPTSA CNDs, L/D-TAMSA CNDs). After reaction, all products were diluted 1000 times and tested by JASCO J815 CD. Additionally, CNDs, CNDs plus (*R*)-(−)-MP under the same conditions as control groups were measured by the same way.

Preparatorily, to study the chirality of CNDs, the hybrid particles (TASA CNDs) were prepared through the hydrothermal processing of sulfanilic acid and racemic tartaric acid (L-TA:D-TA=1:1). Subsequently, the ECD spectra of chiral CNDs and hybrid particles were measured. As shown in Fig. S8a†, no peaks were observed for hybrid particles in the ECD spectra, indicating the achirality of TASA CNDs. This contrasts with L/D-TASA CNDs, which exhibit characteristic absorption peaks.

Next, the chiral catalytic performance of chiral CNDs for ring-opening reaction of racemic SO was investigated. As displayed in Fig. S8b-c†, when L-TASA CNDs catalyze racemic SO, the peak of (*S*)-(+)-MP appears. Conversely, when racemic SO interacts with D-TASA CNDs, the peak of (*R*)-(–)-MP is observed. These results demonstrate that chiral CNDs can catalyze the ring-opening reaction to produce an optically pure product from racemic SO.

7. Catalytic performance of chiral CNDs

The catalytic performance of different chiral CNDs and precursors were studied. Firstly, 120 μL SO and 1.8 mL methanol were added into 4 mL cuvette and stirred at room temperature. Then 450 μL 300 μg/mL of chiral CNDs (L/D-TA CNDs, L/D-TASA CNDs, L/D-TAPTSA CNDs, L/D-TAMSA CNDs) or precursors (L/D-TA, SA, PTSA, MSA) were added into each cuvette, respectively. Then, these cuvettes were immediately sealed and reacted without light for 10 min. At the end, the samples were analyzed by GC with FID and quantified by the internal standard method.

8. The quantification of chiral product of ring-opening reaction

Herein, pure (R)-(–)-MP was selected as a standard substance and the relationship between the concentration of pure (R)-(–)-MP and ECD absorbance was investigate. As shown in Figure S9a†, the absorbance intensity of (R)-(–)-MP at 204 nm increases gradually with the increased concentration of (R)-(–)-MP from 2 to 110 μM. Then, a great linear correlation ($y = – 0.074x – 1.037$) over the range of (R)-(–)-MP from 2 to 110 μM with correlation coefficient squares (R^2) 0.986 are obtained (Figure S9b†).

9. Experimental procedure for reusability tests

The reusability of L-TASA CNDs was evaluated for the ring-opening reaction of SO with methanol under optimized conditions. After each reaction, the heterogeneous mixture was subjected to centrifugation at 24,000 rpm. The catalyst was then separated from the mixture *via* filtering and high-speed centrifugation. The recovered catalyst was reused without further treatment for consecutive runs with fresh SO and methanol. A control group (labeled "blank") was also included, using fresh SO without the addition of chiral CNDs under the same reaction conditions. After the reactions, samples were analyzed by GC with FID detector under the same conditions described above. All experiments were independently repeated for three times (n = 3).

10. Catalytic reaction mechanism of chiral CNDs

To explore the catalytic reaction mechanism and the contribution of the single functional groups of the molecular chromophore on the catalyst performance, different CNDs were synthesized using the same solvothermal procedure. L/D-TA CNDs were synthesized with no additional precursor assisted in evaluating the role of the sulfanilic acid in the catalytic process. L/D-TAPTSA CNDs were prepared with p-toluene sulfonic acid instead of sulfanilic acid. This was meant to evaluate the role of the amine group, which was presumed to be crucial in the amide bond and chromophore formation (*vide supra*). The third reference was synthesized using 4-(methylsulfonyl)anilin instead of sulfanilic acid to investigate the role of the acidic sulfonic functional groups in the catalytic process.

Besides, the optical properties of the different CNDs were studied by means of absorption spectra as well as 3D emission mapping. UV–vis spectra (Fig. S11a†) of different CNDs show that the absorption peaks of TAPTSA CNDs and TAMSA CNDs are located at 221 nm and 261 nm, respectively. The distinct absorbance bands in the near UV area (above 300 nm) are only featuring TASA CNDs and TAMSA CNDs, what proves the formation of the chromophores within the polymeric matrix of the nanomaterial. As can be seen from 3D emission mapping (Fig. S11b-d†), TAMSA CNDs and TASA CNDs show district emission upon excitation between 300 and 400 nm, in contrast to "silent" TA CNDs and TAPTSA CNDs. This can be explained by the fact, that whether TA CNDs nor TAPTSA are able to undergo amidation reaction and form chromophores, responsible for this emission. Furthermore, the fluorescence lifetime and fluorescence quantum yield (FLQY) of chiral different CNDs were analyzed (Table S2†). Noticeably, the FLQY for TASA and TAMSA reaching values of 8.57% and 2.27%, respectively. The aforementioned results revealed that only TA in reaction with MSA/SA as precursors could construct chiral CNDs via one-step hydrothermal method.

Furthermore, the ECD spectra were used to characterize the chirality of the reference CNDs. L/D-TA CNDs maximize at 212 nm (Fig. S12a†). S-chiral CNDs proved to have a positive Cotton effect in the absorption range from 200 to 270 nm, while R-chiral CNDs gave rise to a negative Cotton effect. Similar to L/D-TA CNDs, L/D-TAMSA CNDs, the 215 nm maximum with S-chirality for D-TAMSA CNDs was proven by a positive Cotton effect (Fig. S12b†). In this context, the negative absorbance of L-TAMSA CNDs corroborates the formation of R-chiral CNDs. Compared with the other chiral CNDs, the ECD spectra of L/D-TAPTSA CNDs lacked pronounced features in the same wavelength

range, that is to say, it is too difficult to construct chiral TAPTSA CNDs from chiral TA and PTSA precursors without an ammonia group (Fig. S12c†).

11. Density functional theory (DFT) calculation

In order to investigate the non-covalent interactions of chiral TASA CNDs and SO, the M06-2X functional was utilized for geometry optimization and frequency calculations in aqueous phase ($\varepsilon = 78.36$) with Truhlar's SMD solvent model without any symmetry or geometrical constraints[10]. The def2-SVP basis set was applied for all stationary points. Frequency calculations were operated at the same level to substantiate the stationary points are minimal limit (0 imaginary frequency) and acquire the thermal corrections. Single point energy calculations were implemented at M06-2X/def2-TZVPP level, and empirical dispersion was included for all calculations using the D3 version of Grimme's dispersion[11]. The Gibbs free energies (G) were given by adding free energy corrections from frequency calculations and electronic energies from single point energy calculations. Here, we defined the difference value of G between the chiral CNDs with (*R*)-(–)-SO and (*S*)-(+)-SO as "ΔG", that is "ΔG = G(*R*)-G(*S*)". The initial conformations of all computational models of L/D-TASA CNDs– (*R*)-(–)-/(*S*)-(+)-SO were obtained by sampling all the possible binding models, and the binding pattern with the lowest free energy was reported. Ultimately, computed structures were illustrated by CYLView software. As depicted in Fig. S14a†, ΔG_s of "D-TASA CNDs + (*R*)-(–)-SO" and "D-TASA CNDs + (*S*)-(+)-SO" adducts were calculated as 0 and -1.51 kJ/, respectively. This prompts to the fact that D- TASA CNDs were inclined to react with (*S*)-(+)-SO in contrast to (*R*)-(–)-SO. Similarly, the DFT calculations in Fig. S14b† demonstrate that the obtained ΔG_s for "L- TASA CNDs + (*R*)-(–)-SO" and "L-TASA CNDs + (*S*)-(+)-SO" were -4.34 and 0 kJ/mol, respectively. This suggests that L-TASA CNDs tend to catalyze (*R*)-(–)-SO rather than (*S*)-(+)-SO.

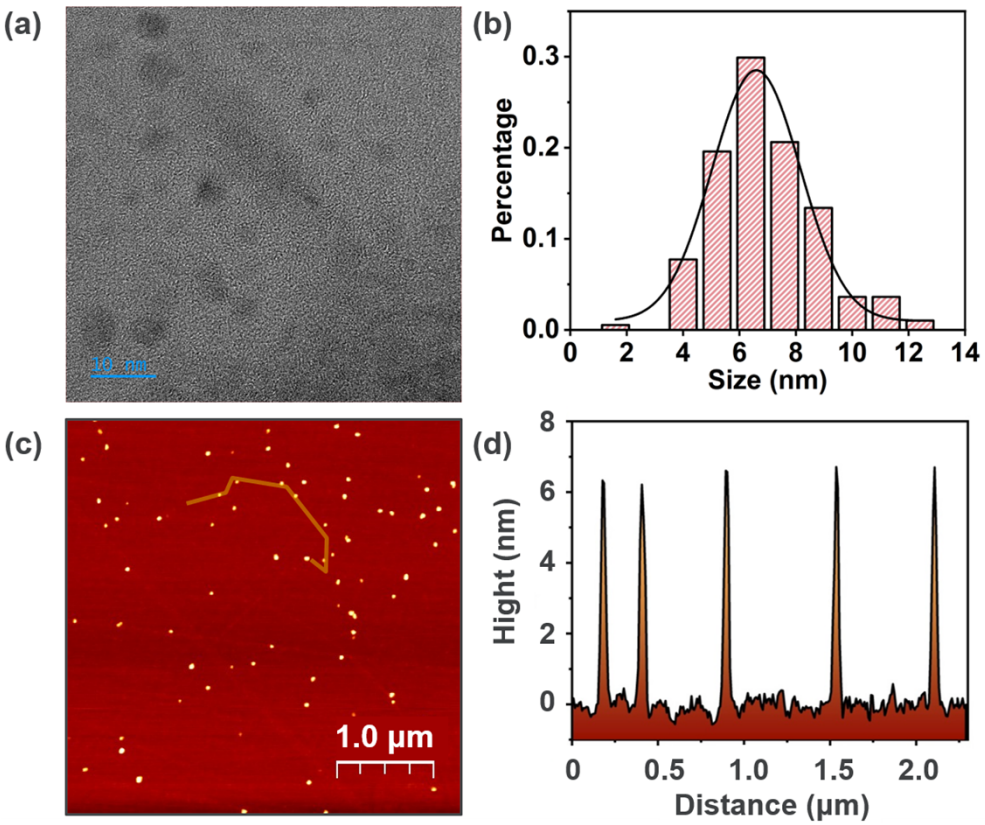

Figure S1. (a) TEM image (scale bar = 10 nm), (b) size distribution, (c) AFM image and (d) statistic average height of synthesized TASA CNDs.

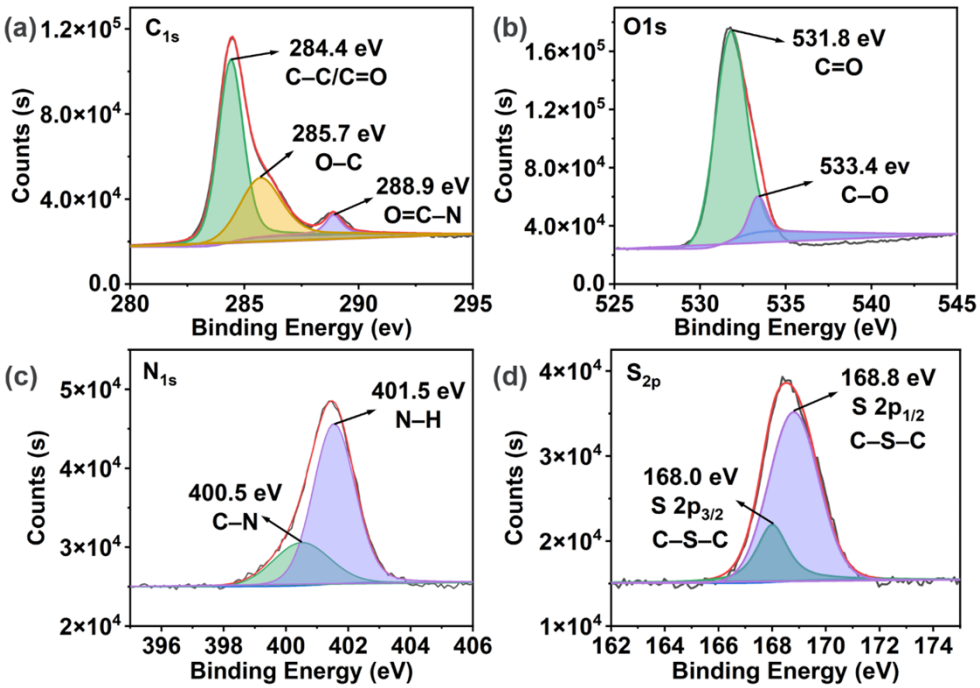

Figure S2. High resolution XPS of (a) C_{1s}, (b) O_{1s}, (c) N_{1s} and (d) S_{2p} of TASA CNDs.

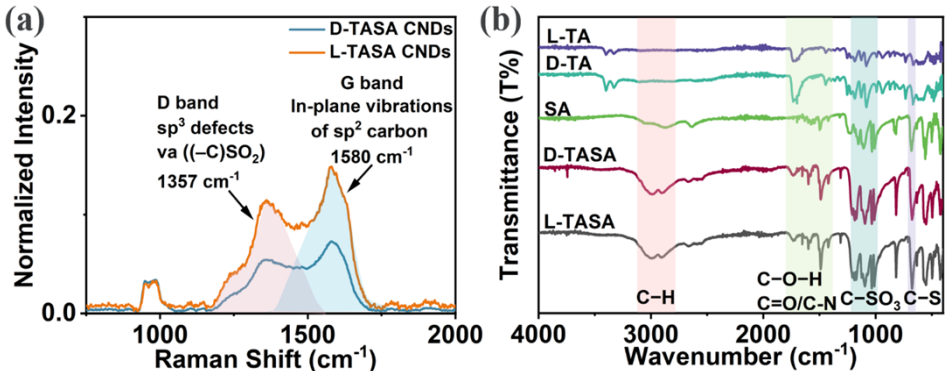

Figure S3. (a) Raman spectra and (b) FTIR spectra of L/D-TASA CNDs.

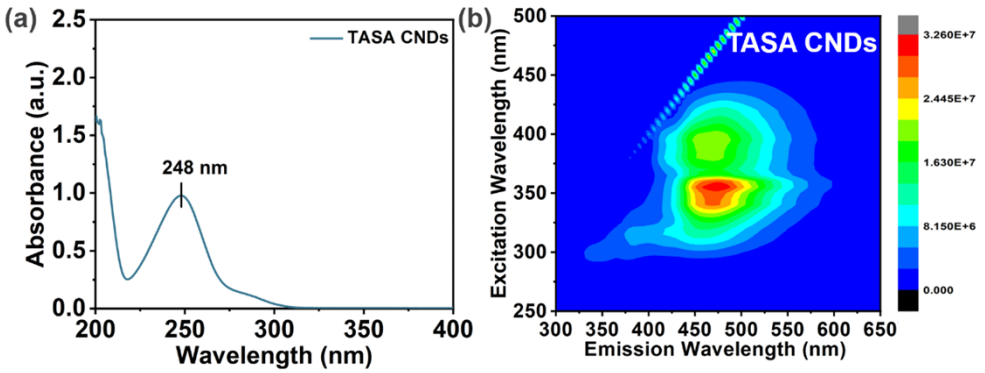

Figure S4. (a) UV–vis absorption and (b) excitation-emission mapping of TASA CNDs.

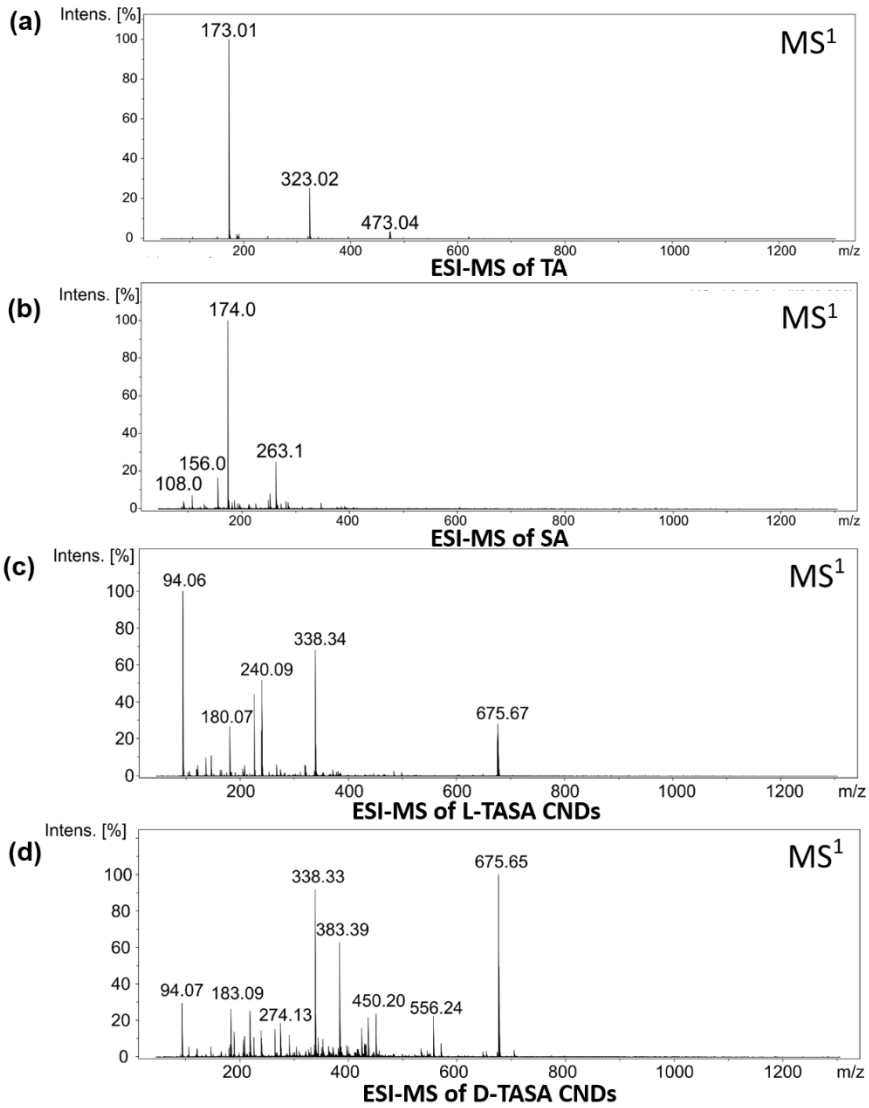

Figure S5. ESI-MS spectra of (a) TA, (b) SA, (c) L-TASA CNDs and (d) D-TASA CNDs.

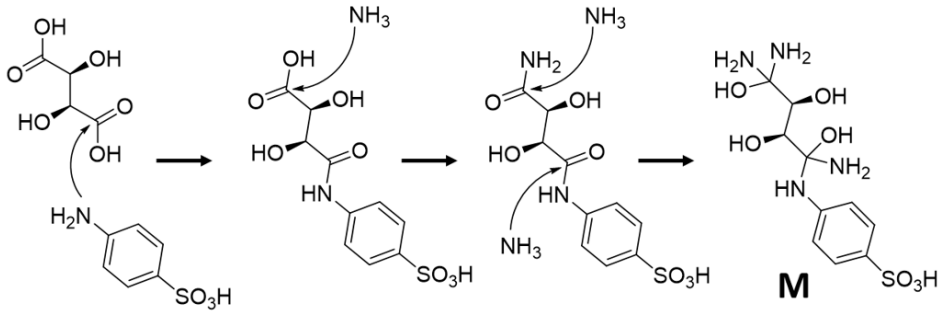

Scheme S1. The feasible modular molecule in preparation process of TASA CNDs.

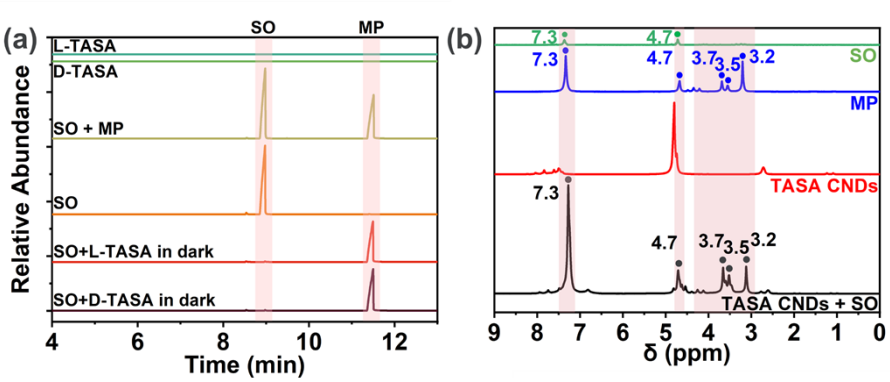

Figure S6. (a) GC spectra of SO, MP, chiral CNDs and the system after catalytic reaction in dark. (b) ^{1}H-NMR spectra of SO, MP, TASA CNDs and the system after catalytic reaction.

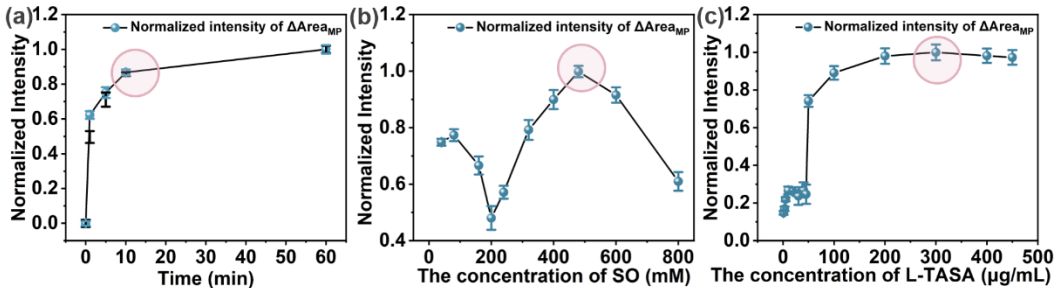

Figure S7. Optimization of (a) reaction time, (b) the concentration of SO, (c) the concentration of L-TASA CNDs (all tests reacted in dark).

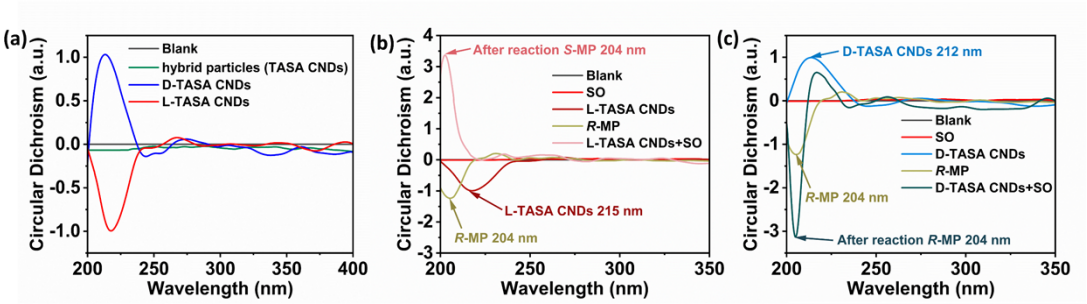

Figure S8. (a) ECD spectra of L/D-TASA CNDs and TASA CNDs. (b, c) ECD spectra before and after ring-opening reaction of racemic SO catalyzed by L/D-TASA CNDs.

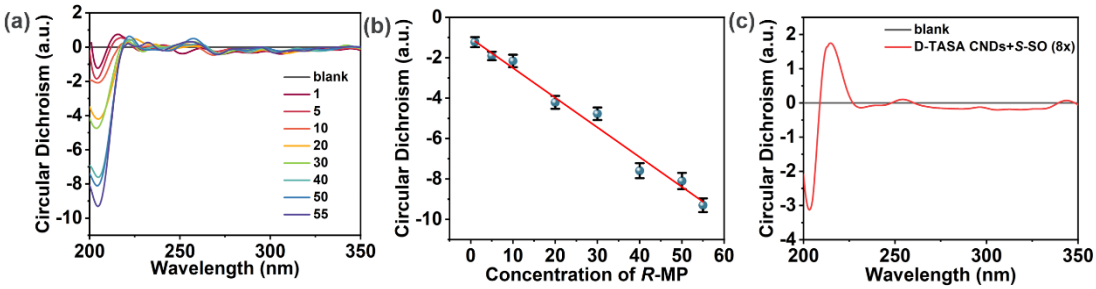

Figure S9. (a) ECD spectra of different concentration of pure (*R*)-(–)-MP (from top to bottom: 0, 2, 10, 20, 40, 60, 80, 100 and 110 μM). (b) Linear relationship between the concentration and CD intensity of pure (*R*)-(–)-MP in ECD spectra. (c) ECD spectra of (*S*)-(+)-SO catalyzed by D-TASA CNDs (the concentration of the system after catalysis reaction was diluted 8-fold).

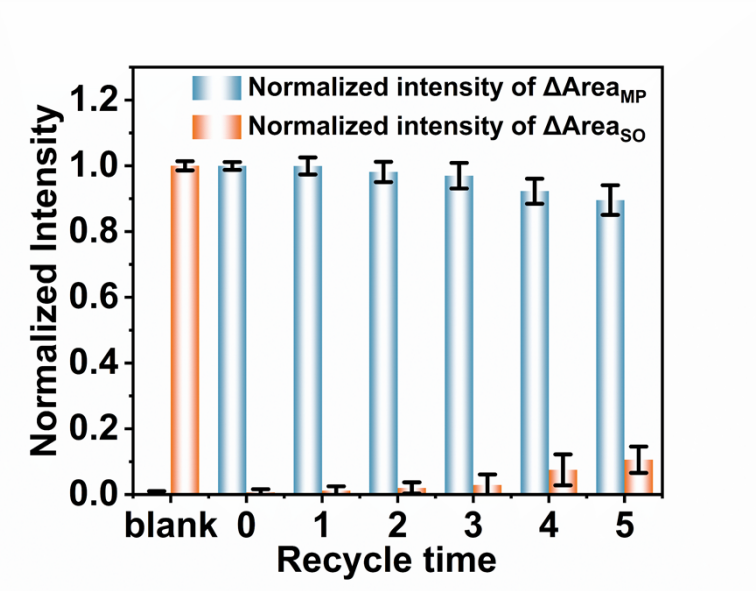

Figure S10. The reusability assay of L-TASA CNDs.

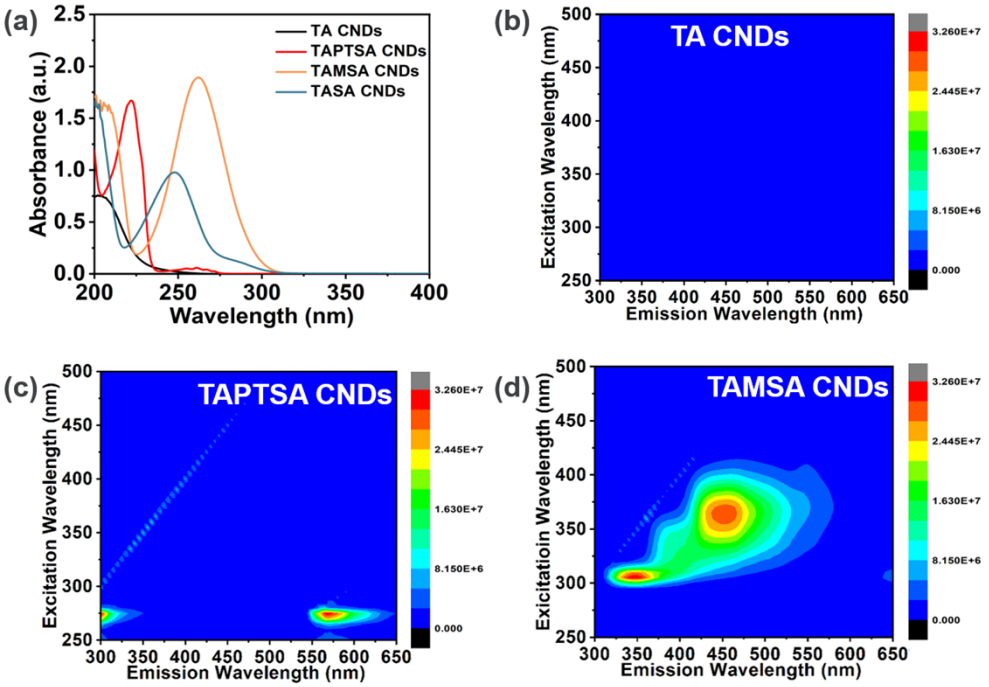

Figure S11. (a) UV–vis absorption and (b-d) excitation-emission mapping of different CNDs.

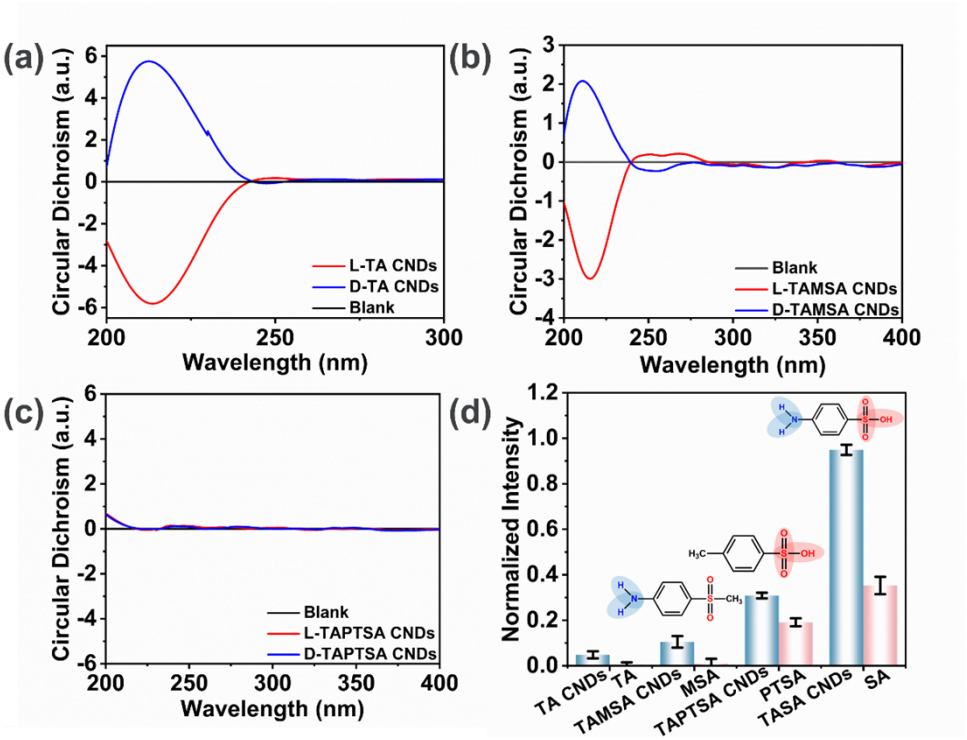

Figure S12. ECD spectra of (a) L/D-TA CNDs, (b) L/D-TAMSA CNDs and (c) L/D-TAPTSA CNDs. (d) Catalytic performance of different CNDs (The structures represent the 2nd used precursor).

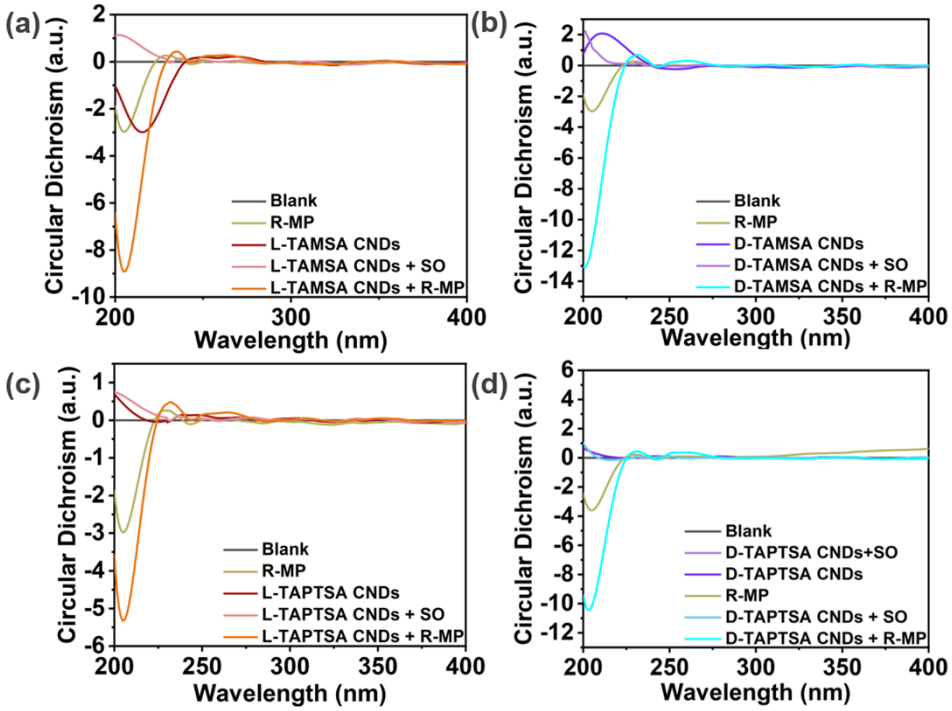

Figure S13. ECD spectra before and after ring-opening reaction catalyzed by (a, b) L/D-TAMSA CNDs and (c, d) L/D-TAPTSA CNDs.

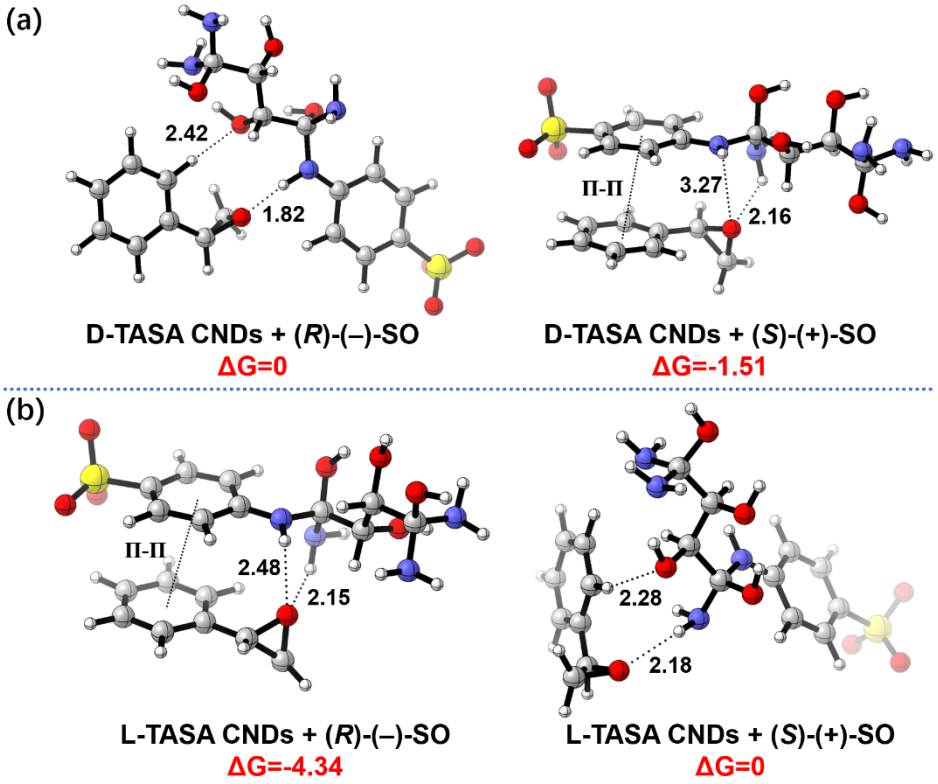

Figure S14. DFT results of (*R*)-(–)-SO/(*S*)-(+)-SO catalyzed by (a) D-TASA CNDs and (b) L-TASA CNDs.

Table S1. The preparation of chiral CNDs by different precursors

First precursor	Second precursor	Name
L/D-Tartaric acid(L/D-TA)	—	L/D-TA CNDs
	Sulfanilic acid (SA)	L/D-TASA CNDs
	P-Toluene Sulfonic acid (PTSA)	L/D-TAPTSA CNDs
	4-(Methylsulfonyl)anilin (MSA)	L/D-TAMSA CNDs

Table S2. Fluorescence lifetime and fluorescence quantum yield of different CNDs

Name	Fluorescence Lifetime	Fluorescence Quantum Yield
TA CNDs	1.39 ns ± 0.01	—
TAPTSA CNDs	2.47 ns ± 0.01	—
TAMSA CNDs	5.48 ns ± 0.01	2.27%
TASA CNDs	7.14 ns ± 0.01	8.57%

Table S3. Comparation of the conversion of ring-opening reaction catalyzed by different chiral CNDs

Name	Conversion	Chiral control (conversion)
L-TA CNDs	4.83%	—
D-TA CNDs	3.56%	—
L-TAMSA CNDs	10.5%	—
D-TAMSA CNDs	8.1%	—
L-TAPTSA CNDs	30.8%	—
D-TAPTSA CNDs	30.2%	—
L-TASA CNDs	99.2%	(*S*)-(+)-MP
D-TASA CNDs	98.3%	(*R*)-(−)-MP

References

1. X. Kou, X. Xin, Y. Zhang and L.-Y. Meng, *Carbon Letters*, 2021, **31**, 695-706.
2. Q. Liu, Z. Dong, A. Hao, X. Guo and W. Dong, *Talanta*, 2021, **221**, 121372.
3. Y. Deng, J. Qian, Y. Zhou and Y. Niu, *RSC Advances*, 2021, **11**, 10922-10928.
4. Y. Cheng, Z. Chen, Y. Wang and J. Xu, *Journal of Photochemistry and Photobiology A: Chemistry*, 2022, **429**, 113910.
5. Y. Reva, B. Jana, D. Langford, M. Kinzelmann, Y. Bo, P. R. Schol, T. Scharl, X. Zhao, R. W. Crisp, T. Drewello, T. Clark, A. Cadranel and D. M. Guldi, *Small*, 2023, **n/a**, 2207238.
6. X. Luo, W. Zhang, Y. Han, X. Chen, L. Zhu, W. Tang, J. Wang, T. Yue and Z. Li, *Food Chemistry*, 2018, **258**, 214-221.
7. A. A. Ensafi, S. Hghighat Sefat, N. Kazemifard, B. Rezaei and F. Moradi, *Sensors and Actuators B: Chemical*, 2017, **253**, 451-460.
8. F. Li, Y. Li, X. Yang, X. Han, Y. Jiao, T. Wei, D. Yang, H. Xu and G. Nie, *Angew. Chem. Int. Ed.*, 2018, **57**, 2377-2382.
9. Y. Reva, B. Jana, D. Langford, M. Kinzelmann, Y. Bo, P. R. Schol, T. Scharl, X. Zhao, R. W. Crisp, T. Drewello, T. Clark, A. Cadranel and D. M. Guldi, *Small*, 2023, **19**, 2207238.
10. P. T. Thuy and N. T. Son, *Journal of Molecular Modeling*, 2021, **27**, 6.
11. Z. Chaughtai, M. A. Hashmi, M. Yar and K. Ayub, *Physical Chemistry Chemical Physics*, 2021, **23**, 8557-8570.